J Seismol (2019) 23:393–401
https://doi.org/10.1007/s10950-018-09812-z

ORIGINAL ARTICLE

Earthquake location by a sparse seismic network

Valerio Materni · Alessandra Giuntini · Rodolfo Console

Received: 11 April 2018 / Accepted: 14 December 2018 / Published online: 24 January 2019

Abstract Hypocentral locations, and depths in particular, are affected by large uncertainties in situations where the available seismic network is sparse and with a small number of local stations recording Pg phases as first arrival (Pg phase is direct wave in the upper crust). In this study, we consider the variability of locations because of the errors associated with arrival time picks, analyzing how this variability, for a constant standard deviation in arrival times, depends on the azimuthal distribution of stations and the number of available Pg phases in the input dataset. Our analysis was carried out on real cases and confirmed the importance of including local stations in the earthquake location process, quantifying how the removal of an increasing number of local stations increased the dispersion of hypocenters.

Keywords Location · Seismic network · Local stations · Pg phases · Dispersion of hypocenters

V. Materni (✉) · A. Giuntini
Istituto Nazionale di Geofisica e Vulcanologia, Via di Vigna Murata, 605, 00143 Rome, Italy
e-mail: valerio.materni@ingv.it

R. Console
Centro di Geomorfologia Integrata per l'Area del Mediterraneo, Via F. Baracca, 175, 85100 Potenza, Italy

1 Introduction

Before the development of digital computers, seismologists were obligated to use long (and often unreliable) manual computations to apply the earthquake location procedure based on the least squares introduced by Geiger (1912). Only in the 1960s did earthquake location programs based on the Geiger's method, such as HYPOLAYR (Eaton 1969) and HYPO71 (Lee and Lahr 1972), became available and popular. Since then, further improvements in location accuracy have come from the growth of the available seismograph networks and the improvement in computing capabilities (see, e.g., Veith 1975; Sambridge and Kennett 1986; Lomax and Curtis 2001).

Even if the increasing computing resources and more sophisticated mathematical tools have provided seismologists with more and more powerful location techniques (such as joint event location (Pujol 2000); source specific station terms (Richards-Dinger and Shearer 2000); double-difference earthquakes location algorithm (Waldhauser and Ellsworth 2000; Console and Giuntini 2006)), it is well known that the accuracy of hypocentral locations is critically conditioned by the density and geometry of the available seismic networks (Myers at al 2000; Bondar et al. 2004). Hypocentral depths, in particular, may be affected by large uncertainties in situations where the available seismic network is sparse and local stations recording Pg phases as first arrival are scarce (Pg phase is direct wave in the upper crust).

This paper is based on the same dataset used by Materni et al. (2015) in their study of teleseismic P wave travel time

corrections estimated for a set of earthquakes located with arrival times reported by the Iranian Seismological Center (IRSC). Comparing the regional locations with teleseismic locations obtained by arrival times reported by the International Seismological Center (ISC), they found location differences of the order of 10–20 km or larger, affecting both epicentral coordinates and depths. Average travel time residuals to each station of the global network were computed for a set of sources located in the study area. They showed that systematic shifts of hypocentral coordinates, as well as the sizes of their error ellipses, can be substantially reduced by applying source-specific station corrections. Their study included an analysis of the effect of removing arrival times of critical stations from the dataset used for the locations, showing that this effect is largely reduced by the application of travel time corrections. In this study, we want to be a little more precise and go into further details about the problem of locating earthquakes by means of P arrival times obtained by a sparse regional network (Fig. 1), using the dataset available from the IRSC in a real case. In particular, we focus here on the variability of locations because of the errors associated with arrival time picks, analyzing how this variability, for a constant standard deviation in arrival times, depends on the azimuthal distribution of stations and the number of available Pg phases in the input dataset.

While the robustness of the epicenter coordinates is mainly controlled by the azimuthal distribution of the recording stations, depth resolution comes from a high variance in the depth derivatives of the travel times. There are, of course, many complicating factors due to the exact geometry of the observing network of stations, but that is the essence of the depth resolution. If the variance of the depth derivatives is zero, the solution matrix is singular and one cannot obtain a depth free solution. As the variance slowly grows, the matrix becomes merely ill-conditioned with poor depth resolution, and finally when the variance is large enough, the matrix can provide a well-constrained depth. The combination of Pg and Pn arrival times can provide some depth control because they are characterized by positive (Pg) and negative (Pn) depth derivatives. Otherwise, either all Pg or Pn arrivals have about the same values for depth derivatives and offer little or no depth control, although a range of distances for Pg would yield some control (Fig. 2).

The depth derivative is cos *i*/V, where *i* is the take-off angle (from vertically downward) and V is the P wave velocity. Therefore, when *i* is zero, the derivative is at its maximum. Consider the simple case of a layer over a half space, with a crustal thickness of about 40 km and velocity of 6 km/s over a half space with velocity of 8 km/s (similar to the velocity model adopted by Materni et al. 2015). Take the source depth to be about 10 km. The Pg arrival that travels in the top layer will come in 1.666 s directly above the source, and its derivative will be 0.1666 s/km. As the distance is increased, the travel time increases and asymptotically approaches the distance/6 km/s line, with a depth derivative that tends to zero (Fig. 2).

The PmP arrival reflected from the second layer directly above the source travels down to the Moho boundary and back up to the surface and arrives at (30 km + 40 km)/6 km/s (i.e., 11.666 s). Its travel time also slowly increases with distance but remains larger than that of the Pg arrival until it reaches the critical angle where the ray is refracted along the interface as a head wave. Beyond this point, the wave is traveling along the boundary at 8 km/s (Pn velocity) with a constant depth derivative of −0.110 s/km. The crossover point where the Pn comes in before the Pg is at about 185 km.

So, when we are dealing with small events where arrivals are limited to Pg and Pn, we have the following limitations; at distances beyond about 60 km, the depth derivatives for Pg are not changing very much; when Pn becomes the first arrival at about 185 km, the depth derivatives do not change at all. Therefore, having travel time observations inside of 60 km greatly improves depth resolution; having both Pg and Pn is a critical condition for depth resolution.

2 Method of analysis

We applied a Monte Carlo method to study the importance of using Pg waves for the robustness of hypocentral locations for two of the earthquakes and the same local/regional seismic network considered by Materni et al. (2015). The selected events are the November 7, 2012 06:26 UTC (M 5.4) and the November 16, 2012 03:58 UTC (M 4.7) earthquakes. The network used in our analysis is composed by 14 stations, but one Pg arrival time is missing at different stations in each of the two events. So the data actually used for the analysis were six Pg and seven Pn arrivals for both events. Two examples of waveform, one with Pg arrival and one with Pn arrival, are displayed in the Fig. 3 for each of events analyzed.

The data are reported in Table 1, and the map showing the epicenters of the events and the station distribution is displayed in Fig. 1. This figure shows that Pg arrivals are

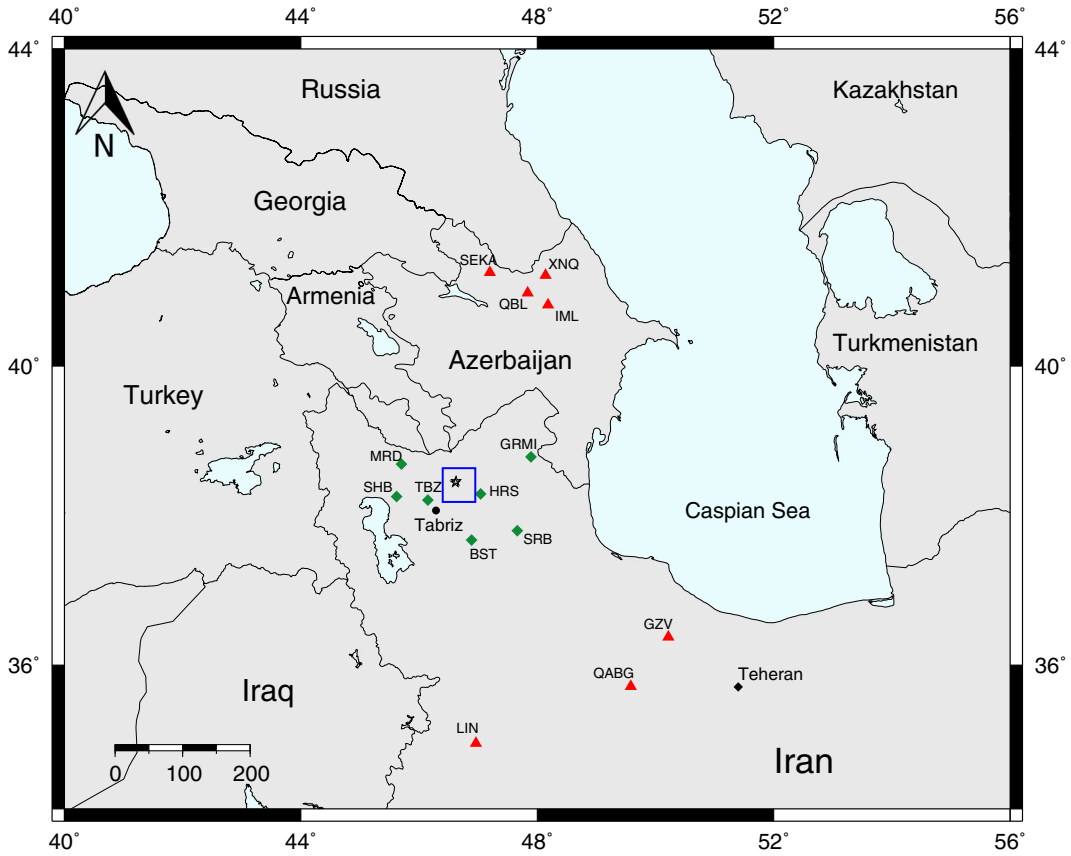

Fig. 1 Geographic framework of the region showing the epicentral area (rectangle), of the two earthquakes analyzed in this study. Diamonds and triangles denote the seismic stations used for event location, respectively for Pg and Pn phases

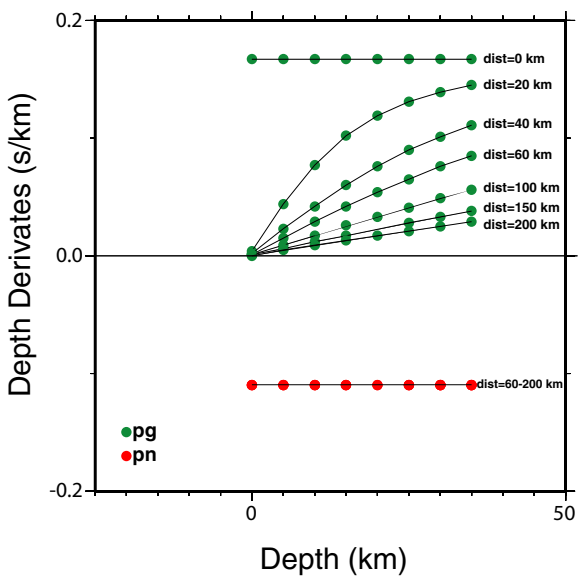

Fig. 2 Trend of the Pg and Pn depth derivates vs depth for a set of epicentral distances

nicely distributed to the east, west, and south, but we only have Pn to the north and south of the epicenters. No S phases were used in our study because they were not present in the real available dataset.

The velocity model used in the location algorithm consists of a single crustal layer of $V_p = 6.13$ km/s velocity and 48.3 km thickness overlying a $V_p = 8.06$ km/s half space (Materni et al. 2015). For our case, the critical angle i_c is 48.59°. Due to the simplicity of the velocity model adopted in this exercise, we assumed that Pg phases can only leave the hypocenter in upgoing direction.

First, we computed the location of the events by means of the 13 observed arrival times for P waves by means of the same location code and applying the same station travel time corrections as in Materni et al. (2015). This algorithm provides also the RMS of the residuals for all the arrival times and the error ellipse parameters.

Using the hypocentral coordinates obtained in this way (Table 2), we computed the theoretical arrival times at every station for each of the two selected events

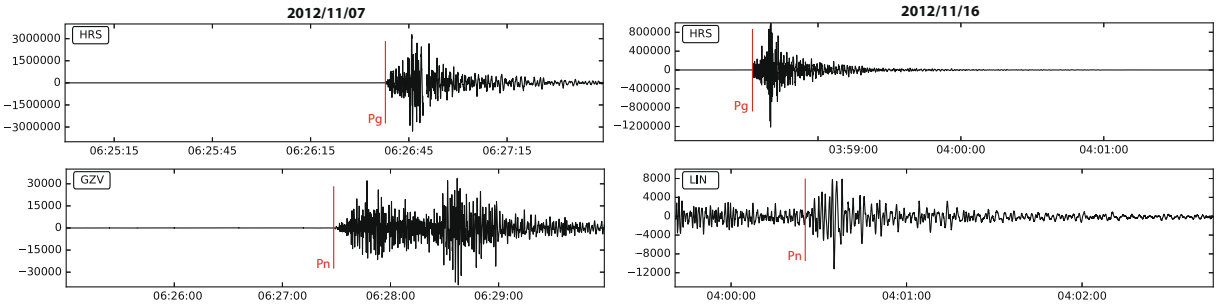

Fig. 3 Example of Pg and Pn arrivals for the November 7, 2012 event on the left and for the November 16, 2012 event on the right

(Table 1). As a consistency check, we verified that the location code applied to the theoretical travel times leads to the same hypocentral coordinates and origin time from which the computation of the theoretical arrival times was started, within the computer precision.

By means of a simple computer code, we created a file of 1000 sets of synthetic arrival times by altering the theoretical travel times with a random value having zero mean and the same RMS as the real residuals. We carried out this simulation assuming an RMS equal to 0.33 s and 0.39 s respectively for the two earthquakes considered in this analysis (Table 2).

The input files containing 1000 sets of synthetic arrival times were processed by the usual location code, obtaining 1000 sets of hypocentral coordinates for each earthquake.

The process of creating 1000 sets of random arrival times was repeated removing from every set 2, 4, 5, and 6 Pg arrivals, systematically starting from the closest station to the farthest. For each of these cases, the locations were carried out again, except for the last case of no Pg in the data sets, for which the location process became unstable and stopped frequently because of inverse matrix singularities, as expected.

3 Results

The results of the analysis are displayed in Figs. 4, 5, 6, and 7 showing the epicentral maps and the vertical cross

Table 1 Observed and theoretical arrival times for each of the seismic stations used for the two events analyzed in this study

Station	Phase	Event (November 7, 2012)				Event (November 16, 2012)			
		Az (°)	Epicentral distance (km)	Time observed (hh:mm:ss.ss)	Time theoretical (hh:mm:ss.ss)	Az (°)	Epicentral distance (km)	Time observed (hh:mm:ss.ss)	Time theoretical (hh:mm:ss.ss)
HRS	Pg	104	42.4	06:26:37.80	06:26:37.69	106	42.4	03:58:32.50	03:58:32.26
TBZ	Pg	179	48.0	06:26:38.10	06:26:38.47	178	49.1	03:58:33.20	03:58:33.35
MRD	Pg	350	82.7	06:26:44.30	06:26:44.04	349	82.6	03:58:38.70	03:58:38.67
SHB	Pg	192	88.2	06:26:45.10	06:26:45.00	191	89.4	03:58:40.00	03:58:39.82
SRB	Pg	113	118.4	06:26:49.70	06:26:49.88	–	–	–	–
BST	Pg	–	–	–	–	135	91.6	03:58:39.70	03:58:40.19
GRMI	Pg	78	119.5	06:26:50.50	06:26:49.92	78	118.4	03:58:44.80	03:58:44.28
IML	Pn	51	292.6	06:27:15.80	06:27:15.79	51	290.4	03:59:10.00	03:59:10.27
QBL	Pn	47	296.0	06:27:15.80	06:27:16.19	47	293.7	03:59:10.80	03:59:10.67
SEKA	Pn	40	309.4	06:27:17.80	06:27:17.89	39	307.2	03:59:12.20	03:59:12.38
XNQ	Pn	48	328.4	06:27:20.00	06:27:20.28	48	326.2	03:59:14.20	03:59:14.77
GZV	Pn	111	397.7	06:27:28.30	06:27:28.74	111	397.7	03:59:23.30	03:59:23.54
QABG	Pn	119	407.7	06:27:29.60	06:27:30.08	119	408.9	03:59:24.20	03:59:24.94
LIN	Pn	142	397.7	06:27:30.00	06:27:28.97	142	399.9	03:59:25.00	03:59:23.95

Table 2 Origin time with RMS, hypocentral coordinates with 1σ depth uncertainty and 90% confidence level error ellipse parameters obtained by 13 observed P waves arrival times. RMS, travel time residual; Smax, major semi axis of the error ellipse; Smin, minor semi axis of the error ellipse; Az, azimuth

	Time (hh:mm:ss.ss)	RMS (s)	Lat (°)	Long (°)	Depth (km)	Smax (km)	Smin (km)	Az (°)
Event (November 7, 2012)	06:26:30.55	0.33	38.479	46.601	10.0 ± 1.5	2.37	2.01	113
Event (November 16, 2012)	03:58:25.16	0.39	38.497	46.614	8.7 ± 1.9	2.73	2.49	51

sections for the earthquakes of November 7, 2012 and November 16, 2012 respectively. The four panels of each figure represent the results obtained using the whole set of 13 arrival times or the results obtained after having removed 2, 4, and 5 Pg arrivals in each of them. Each panel shows the location obtained with the observed dataset, by a star, and the 1000 locations obtained randomly changing the theoretical arrival times at a time, by diamonds. The epicentral maps shown in Figs. 4 and 5 display also the 90% confidence level error ellipse estimated by the assumption of an RMS equal to 0.33 s and 0.39 s for the two events respectively.

As the results are quite similar for both events of November 7, 2012 and November 16, 2012, we proceed with the discussion considering the two events together.

The epicentral maps (Figs. 4 and 5) show a nearly circular geometric distribution of the 1000 locations with a diameter of about 6 km, obtained by the full set of 13 stations. Almost the same situation is obtained after having removed two Pg arrivals from the respective data set. This is obviously a consequence of the good azimuthal distribution of the network of stations, which achieves a limited azimuthal gap.

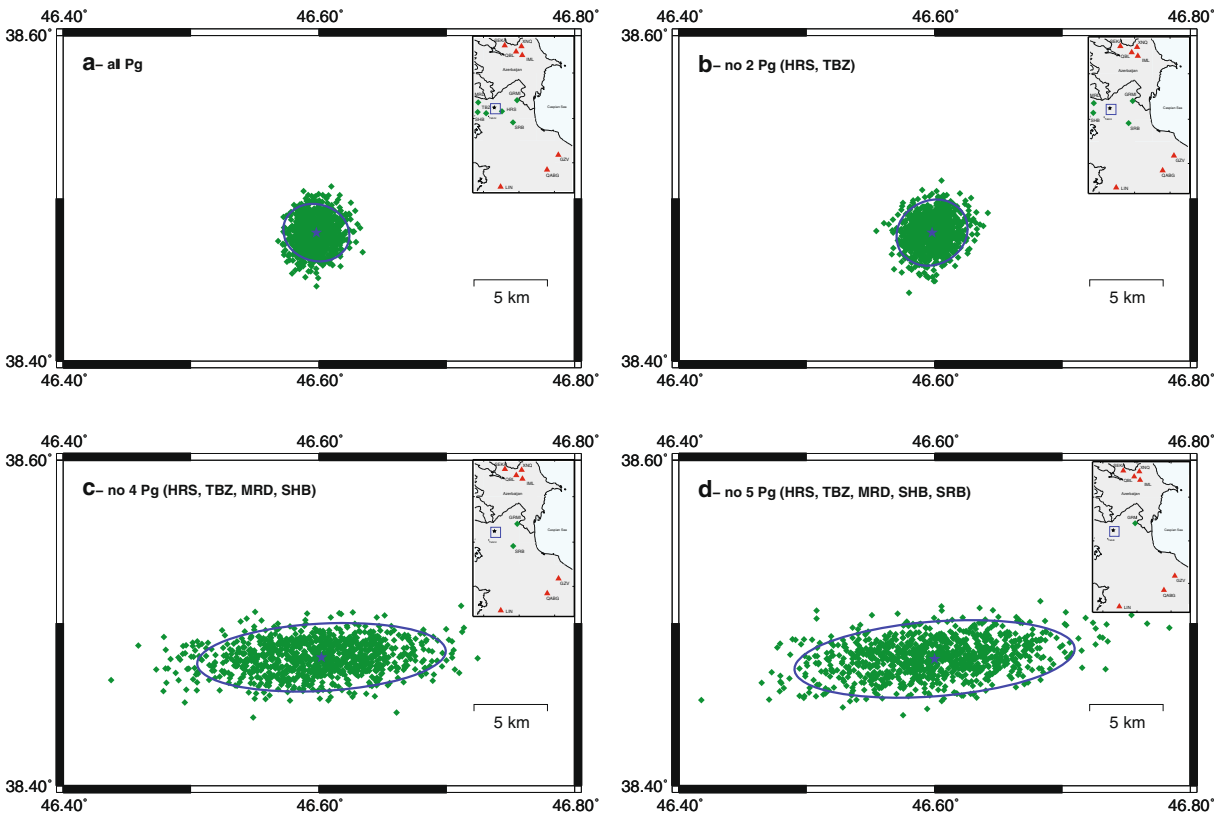

Fig. 4 Epicentral locations obtained for the event of November 7, 2012 by the full set of 13 stations (**a**) and after having removed 2 (**b**), 4 (**c**), and 5 (**d**) Pg arrivals respectively. The star denotes the epicenter reported in Table 1

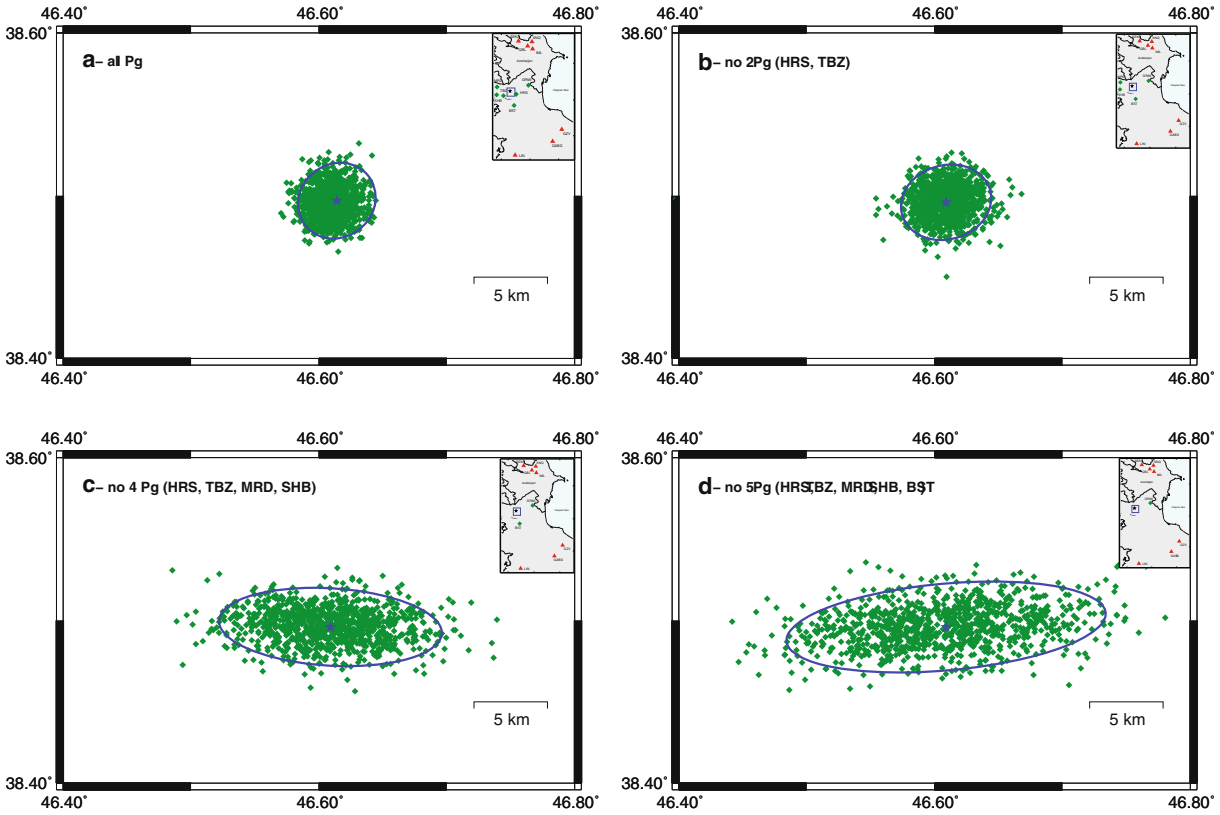

Fig. 5 As in Fig. 4, for the event of November 16, 2012

Proceeding with the removal of two more Pg stations from the datasets of both events, we can notice that the dispersion of the 1000 epicenters becomes quite elongated in E–W direction assuming a length of about 30 km, and this effect is increased further by the removal of one more station, leaving only one Pg arrival in the datasets. Clearly, in these two cases, the uneven azimuthal distribution of stations, leaving an azimuthal gap larger than 180° to the west of the epicentral area, causes a strong trade-off between the horizontal location of the earthquakes and their origin time (Figs. 4 and 5). In these cases, the remaining stations, almost all of which observing Pn phases, are located only to the north and the south of the events, causing the above mentioned strong E–W elongation of the epicenters.

Moving to the vertical hypocenter cross sections (Figs. 6 and 7), we can soon notice that, even with the full datasets of 13 arrival times, they show an elliptical shape elongated along a direction dipping about 15–20° from the vertical towards the west. This trend is maintained with the removal of the two closest stations receiving a Pg phase as first arrival. It is, as expected, the effect of the trade-off between depth and origin time. With the removal of two more Pg arrivals, this effect is much enhanced, but with a trend of the dispersion dipping about 45° towards the East. In these cases, we must account for a trade-off among horizontal coordinates, depth and origin time at the same time. The largest dispersion of the two cases without four or five Pg arrivals results in negative depths (which are fixed to 1 km by the location code) for some of the 1000 random datasets. However, this circumstance does not have effect on the horizontal position of the epicenters.

4 Discussion

For comparison with the results obtained by the Monte Carlo simulations, we computed the 90% confidence level error ellipses of the locations of both events using the observed arrival times reported in Table 1 and corrected for the systematic station residuals. The error ellipses so obtained are reported in Table 2 and shown in Figs. 4 and 5. This test shows a good match between the

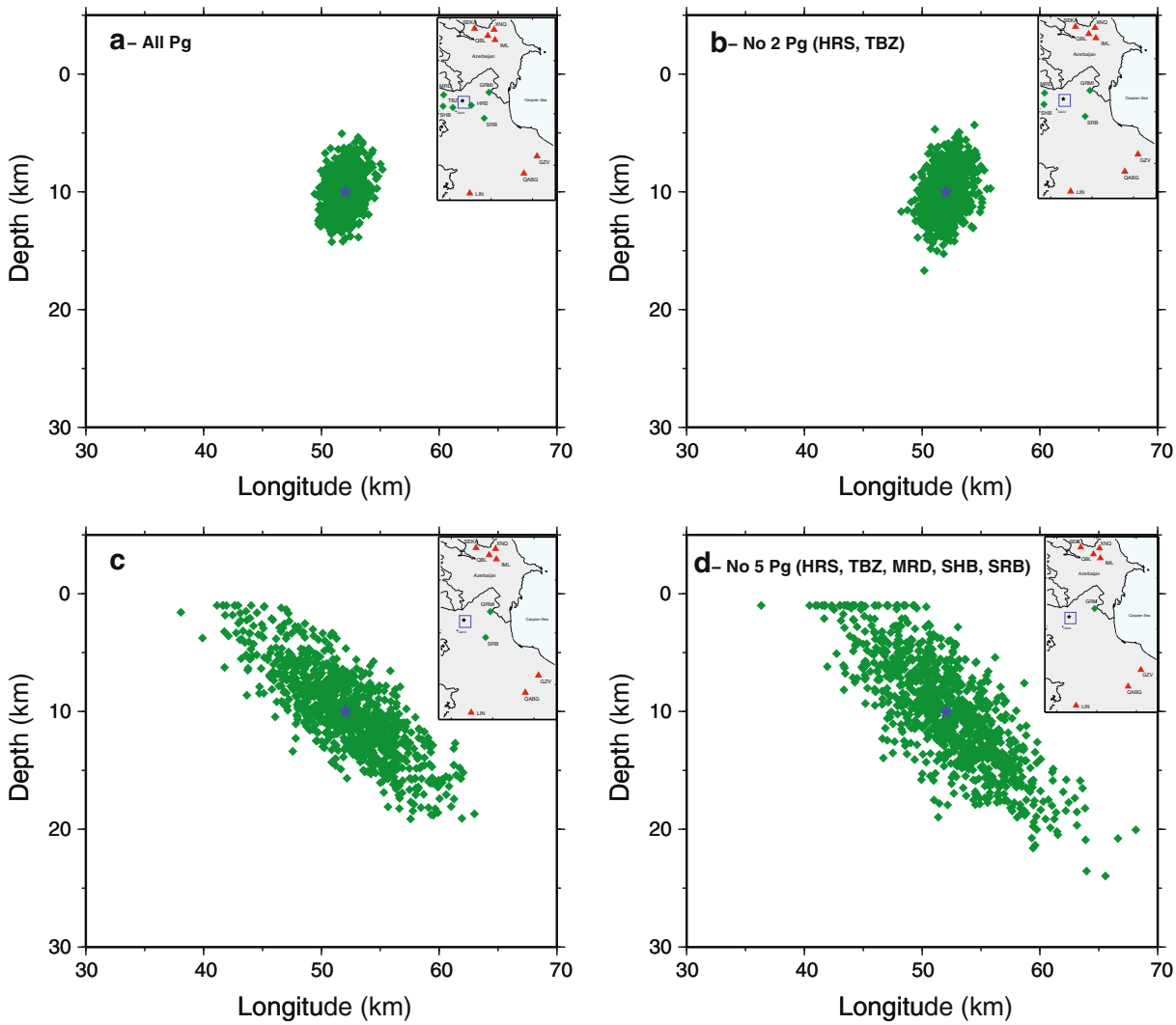

Fig. 6 Vertical sections obtained for the event of November 7, 2012 by the full set of 13 stations (**a**) and after having removed 2 (**b**), 4 (**c**), and 5 (**d**) Pg arrivals respectively. The star denotes the hypocenter reported in Table 1

shapes of the epicentral dispersions obtained by the Monte Carlo method and the error ellipses computed theoretically from the station distribution. There is a mathematical explanation for this match, as described in the following (Veith, personal communication).

The inverse location matrix used to locate any hypocenter describes a four-dimensional probability density function for the hypocenter. The general shape is specified by the locating network and the particular earth model that is used in the location of that particular event. The size is controlled by the variance of the data. If we connect the points of equal probability density, we obtain a hyperellipsoid. Integrating outward from the center (the hypocenter location and point of highest probability density) along surfaces of equal probability density, we get figures describing the configuration of the uncertainty at any limiting confidence level. When we compute the 90% confidence ellipse, what we have done is to integrate the probability density function over all source depths and all source times to project all the uncertainty onto the latitude-longitude plane. The 90% confidence ellipse then specifies the figure that should contain 90% of the hypocenters made with that particular network at the particular variance value. So, Figs. 4 and 5 precisely describe the uncertainty field for the individual networks at the variance level given by RMS of the data. Since we neglect the Pg stations in a specific order, the changes as one goes from a to b, to c, and to d in those figures are a result of the change in the

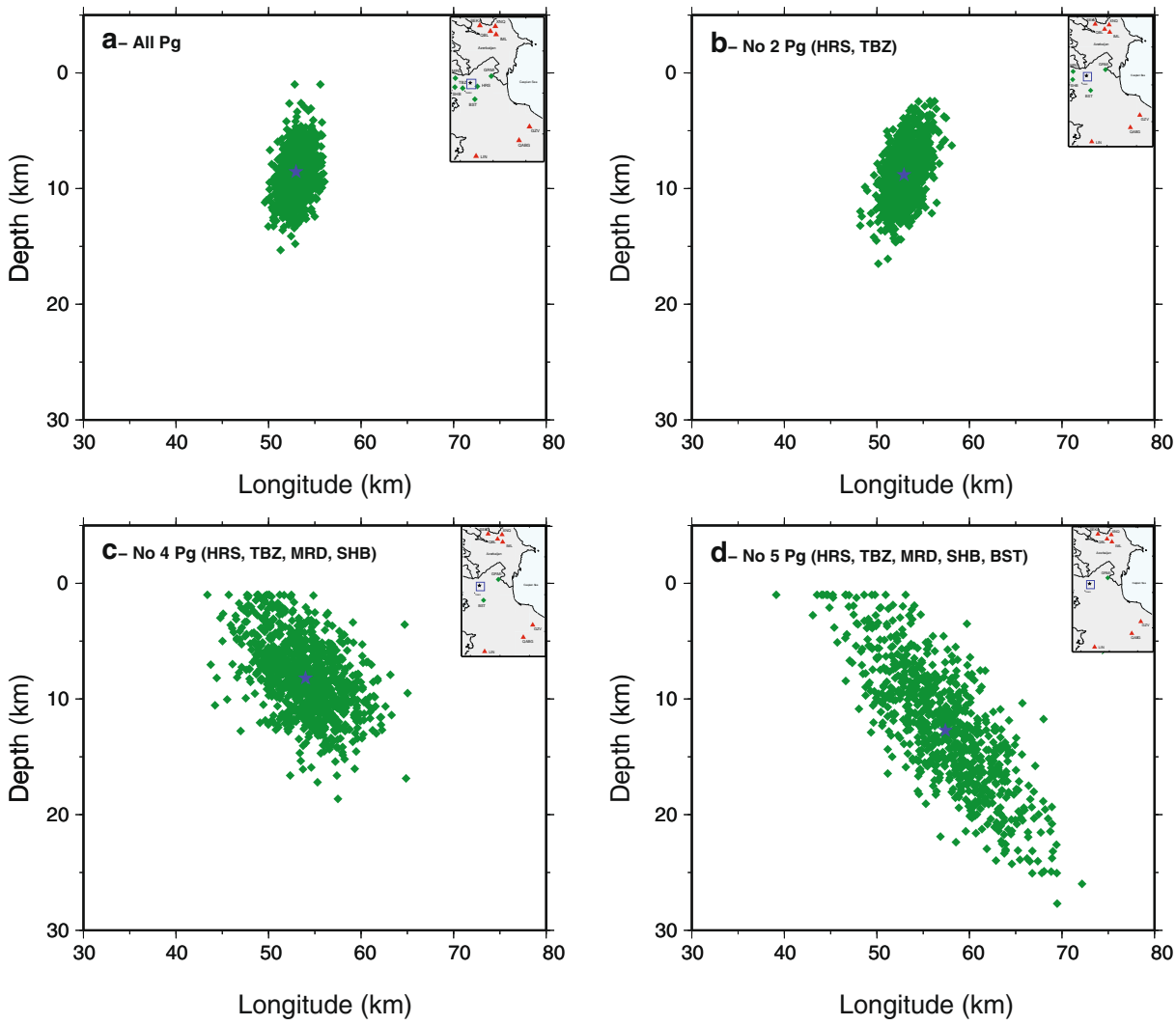

Fig. 7 As in Fig. 6, for the event of November 16, 2012

locating network (the network RMS was not changed). These changes are not smooth; they are purely a result of changing the network geometry, increasing both the minimum epicentral distance and the azimuthal gap step by step, hence the change in orientation of the hypocenters in Figs. 6 and 7 as one goes from b to c.

5 Conclusions

The results of our analysis have highlighted, as expected, the importance of including local stations in the earthquake location process; the removal of an increasing number of local stations increased the dispersion of hypocenters. This study has demonstrated how in the transition from the locations with six Pg phases to the cases with only four, two, and one Pg phases, the 90% confidence ellipses grow in their dimensions as the solution matrix becomes more ill-conditioned.

Acknowledgements We are grateful to Karl F. Veith for his invaluable comments and suggestion in the preparation of this article, with particular reference to the "Introduction" and "Discussion." We thank also three reviewers for constructive remarks which have significantly contributed to the improvement of our manuscript.

Data and Resources

Arrival times and waveforms for the events of the cluster have been obtained from the Iranian Seismological Center (IRSC, http://irsc.ut.ac.ir/; last accessed December 2013). The plots were

performed using the GMT—Generic Mapping Tools version 4.5.9 (www.soest.hawaii.edu/gmt ; Wessel and Smith, 1998).

References

Bondar I, Myers SC, Engdahl ER, Bergman EA (2004) Epicentre accuracy based on seismic network criteria. Geophys J Int 156:483–496

Console R, Giuntini A (2006) An algorithm for double difference joint hypocenter determination application to the 2002 Molise (Central Italy) earthquake sequence. Ann Geophys 49:841–852. https://doi.org/10.4401/ag-3134

Eaton JP (1969) HYPOLAYR, a computer program for determining hypocenters of local earthquakes in an earth consisting of uniform flat layers over a half space. Open file report, U.S. Geological Survey. https://pubs.er.usgs.gov/publication/ofr6985

Geiger L (1912) Probability method for the determination of earthquake epicenters from the arrival time only. (translated from Geiger's 1910 German article: Herbsetimmung bei Erdbeben aus den Ankunfzeiten. K. Gessell. Wiss. Goett. 4, 331-349). Bulletin of St. Louis University 8(1):56–71

Lee WHK, Lahr JC (1972) HYP071: a computer program for determining hypocenter, magnitude, and first motion pattern of local earthquakes. Open file report, U. S. Geological Survey. https://pubs.er.usgs.gov/publication/ofr72224

Lomax A, Curtis A (2001) Fast, probabilistic earthquake location in 3-D models using oct-tree importance sampling. Geophys Res Abstracts, 3:955. http://alomax.free.fr/abstracts/egs_2001_abs.html

Materni V, Giuntini A, Chiappini S, Console R, Chiappini M (2015) Relocation of earthquakes by source-specific station corrections in Iran. Bull Seismol Soc Am 105(5):2489–2509. https://doi.org/10.1785/0120140346

Myers SC (2000) Improving sparse network seismic location with bayesian kriging and teleseismically constrained calibration events. Bull Seismol Soc Am 90(1):199–211

Pujol J (2000) Joint event location—the JHD technique and applications to data from local seismic networks. In: Thurber CH, Rabinowitz N (eds) Advances in seismic event location. Kluwer Academic Publishers, Dordrecht

Richards-Dinger KB, Shearer PM (2000) Earthquake locations in southern California obtained using source specific station terms. J Geophys Res 105:10939–10960

Sambridge M, Kennett BLN (1986) A novel method for hypocentre location. Geophys J R Astron Soc 87:679–697

Veith KF (1975) Refined hypocenters and accurate reliability estimates. Bull Seismol Soc Am 65:1199–1222

Waldhauser F, Ellsworth WL (2000) A double-difference earthquake location algorithm: method and application to the northern Hayward fault, California. Bull Seismol Soc Am 90:1353–1368